

# Tensile Decohesion by Local Failure Criteria

T. Siegmund, W. Brocks

*Debonding of two elastic-plastic blocks by a ductile failure mechanism is investigated. The bond line between the two blocks is specified either as a strip of a material described by the modified Gurson relation or by a cohesive zone model. The cohesive zone material parameters are deduced from analyses of void containing unit cells apart from the debonding analysis. Here, the behavior of the material is described by the modified Gurson model. The present computations of debonding show that the external stress biaxiality imposed on a specimen has important implications on the agreement between the predictions of the two models. At high level of external stress biaxiality the predicted debonding behavior is influenced little by changes in the loading conditions. The cohesive zone parameters as deduced from uniaxial straining lead to good agreement with the predictions of the Gurson model. At low levels of applied stress biaxiality the debonding behavior is strongly dependent on a change in external loading and an a priori choice of cohesive material parameters was not possible.*

## 1 Introduction

An essential ingredient of material modeling aimed to characterize material failure is that the constitutive description of the material under consideration has to allow that the deformation localizes or that the material can lose its capacity to transmit stresses. If material failure is due to ductile tearing – i.e. induced by void growth and void coalescence – there exist two approaches to the modeling of material separation. In both approaches the zone where material degradation takes place is termed process zone which is embedded in a material that does not fail.

One approach that can mirror the local loss of stress carrying capacity is the introduction of a cohesive zone where the tractions in the process zone are related to the magnitude of material separation. Such a type of a traction–separation law has been introduced by Barenblatt (1962) and possesses mainly two material parameters, a cohesive strength and a cohesive energy. This model has become attractive again recently for a series of applications in the computational modeling of fracture. Applications of cohesive models to ductile fracture include the simulation of quasistatic loading, Needleman (1990a,1990b), Tvergaard et al. (1992, 1994, 1996), Yuan et al. (1996), Siegmund et al. (1997) and dynamic loading, Siegmund et al. (1997), as well as the application to bimaterial systems, Siegmund et al. (1997), and composite materials, Needleman (1987), Tvergaard (1993), Finot et al. (1994). These applications demonstrate that the trends predicted by the application of a cohesive zone model are quite sensitive to the choice of the cohesive zone parameters. Only relatively small changes in the parameter values may result in a strong variation of the predicted specimen response.

An alternative way for the analysis of crack growth is the use of the Gurson constitutive equation and its modification, Needleman et al. (1984). This approach incorporates several of the physical details of the micromechanisms of failure into the material's constitutive equation: this is an initial void volume fraction, void nucleation and growth, as well as final void coalescence. This approach has successfully been applied by numerous authors, e.g. Needleman et al. (1987), Sun et al. (1992), Brocks et al. (1995), Xia et al. (1995), Ruggieri et al. (1997), to investigate the propagation of cracks in ductile materials in various specimen geometries. The recent work of Xia et al. (1995) and Ruggieri et al. (1997) demonstrate an interesting approach on how this constitutive equation can easily be connected with a microstructural length scale.

In the first part of the paper the cohesive zone material parameters are determined by the use of the modified Gurson constitutive equation. Special consideration is given to the influence of the triaxiality of the stress state on the cohesive material parameters.

In the second part the problem of decohesion of two blocks is analyzed, Needleman (1990a,1990b). The geometry of the specimen under investigation is depicted in Figure 1a. The process zone bonding the two blocks together is described in two different ways, see Figure 1b: (1) by the use of a cohesive zone model and (2) by the use of the modified Gurson constitutive equation. Here, the material parameters

for the cohesive model are deduced from the model material used in (2). Both models have in common that a length scale is introduced into the calculation and that the stresses in the process zone are limited in their magnitude.

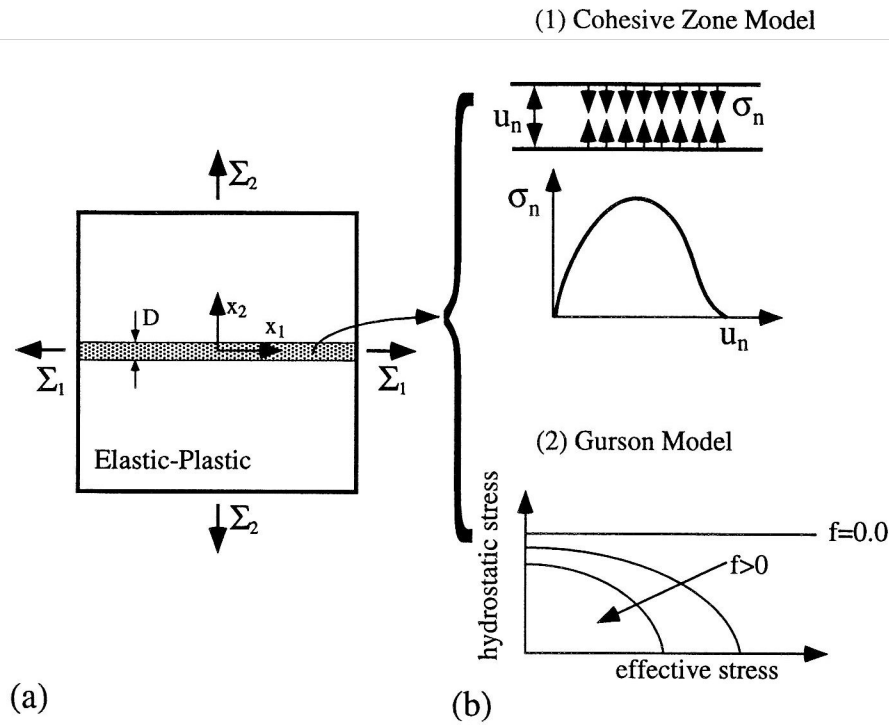


Figure 1. (a) The Specimen under Consideration. The Bonding Region of Height  $D$  is the Region in which Material Failure is Allowed to Occur. (b) Visualization of the Two Approaches Used for the Description of the Bonding Region: (1) the Cohesive Zone Model and (2) the Gurson Model

Having in mind that both models are intended as predictive tools in computational fracture mechanics it is the intention of this investigation to compare the calculated behavior of the two approaches. Limitations of the applicability of the two models are sought.

## 2 The Cohesive Zone Parameters

The separation of two material blocks along a predefined process zone can be described by use of a cohesive zone model. The present study uses the traction–separation relation of Needleman (1990a). This model is shortly reintroduced in the following.

The simulation of pure mode I crack growth is considered and only normal separation along the assumed crack path occurs. The traction–displacement relation (Figure 2) then reads:

$$\sigma_n = \sigma_{max} e^{-z \frac{u_n}{\delta}} \exp\left(-z \frac{u_n}{\delta}\right) \quad (1)$$

Here,  $\sigma_n$  is the normal traction at the crack plane and  $u_n$  is the displacement jump across the crack, i.e. the crack tip opening displacement.  $z = 16e/9$  and  $e = \exp(1)$ .  $\delta$  is the characteristic length of the cohesive zone model and  $\sigma_{max}$  is the maximum value that is reached by  $\sigma_n$ . The cohesive energy,  $\Gamma$ , for this traction–displacement relation equals

$$\Gamma = \frac{9}{16} \sigma_{max} \delta \quad (2)$$

For the present formulation the main portion of energy is spent between  $u_n = 0$  and  $u_n = \delta$ . It now

remains to determine two of the cohesive material parameters, either  $\sigma_{max}$ ,  $\Gamma$  or  $\delta$ , for the material under consideration.

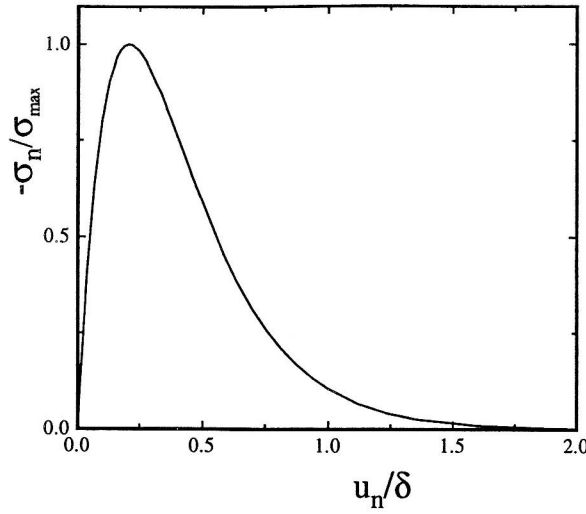


Figure 2. The Traction Separation Law Used

With reference to Tvergaard et al. (1992) the modified Gurson model, see e.g. Needleman et al. (1984), is used to predict the traction-displacement law for a material that fails by the growth of voids and coalescence of voids. A material element of size  $D \times D$  is taken out of the process zone. This material element is analyzed in plane strain under a homogeneous stress-strain state. The yield function of the modified Gurson relation used in the present context is

$$\Phi = \left( \frac{\sigma_e}{\sigma_M} \right)^2 + 2q_1 f^* \cosh \left( \frac{3}{2} \frac{q_2 \sigma_h}{\sigma_M} \right) - \left[ 1 + q_3 (f^*)^2 \right] = 0 \quad (3)$$

Here,  $\sigma_e$ , is the von Mises stress and  $\sigma_h$  the hydrostatic stress acting on the material cell.  $\sigma_M$  is the flow strength of the material surrounding the void. The uniaxial strain stress response of the elastic-plastic material that surrounds the void is described by

$$\epsilon = \sigma / E \quad \text{for } \sigma \leq \sigma_0 \quad (4)$$

$$\epsilon = (\sigma_0 / E) (\sigma / \sigma_0)^{(1/N)} \quad \text{for } \sigma \geq \sigma_0 \quad (5)$$

where  $E$ ,  $\sigma_0$ ,  $N$  denote elastic modulus, yield strength of the material and strain hardening coefficient, respectively. The material properties are taken to be  $E/\sigma_0 = 500$  and  $N = 0.1$ . Poisson's ratio is  $\nu = 0.3$ . The values of the parameters,  $q_1, q_2, q_3$ , used for the modified Gurson relation are  $q_1 = 1.5, q_2 = 1.0, q_3 = q_1^2$ . The effect of void coalescence and final loss of stress carrying capacity is captured by using the modified volume fraction,  $f^*$ . Here,  $f^*(f)$  is taken as a bilinear function of  $f$ :  $f^*(f) = f$  for  $f \leq f_c$  and  $f^*(f) = f_c + k(f - f_c)$  for  $f > f_c$ . Final failure occurs if the condition  $f^*(f_f) = 1/q_1$  is reached. In the following attention is focussed on preexisting voids only. All calculations were performed for  $f_0 = 0.005, f_c = 0.15, k = 5.16$ .

In one set of calculations the loading of the cell is performed under various constant overall true stress ratios,  $\rho$ , see Figure 3a,

$$\rho = \frac{\sigma_1}{\sigma_2} \quad (6)$$

Furthermore, the boundaries of the cell remain straight and parallel to their initial configuration. For plane strain and incompressible material behavior the stress ratio,  $\rho$ , prescribed to the computational

cell is related to the triaxiality,  $T$ , by

$$T = \frac{1}{\sqrt{3}} \frac{1+\rho}{1-\rho} \quad (7)$$

The behavior of the material cell was investigated for applied stress ratios  $\rho = 0.27, 0.44, 0.55, 0.68, 0.75, 0.79$ . These values correspond to applied stress triaxialities of  $T = 1.0, 1.5, 2.0, 3.0, 4.0, 5.0$ . An additional calculation was performed for the condition of uniaxial straining, Figure 3b. This boundary condition is the same as used in Tvergaard et al. (1992) for the determination of the material parameters for their cohesive zone model.

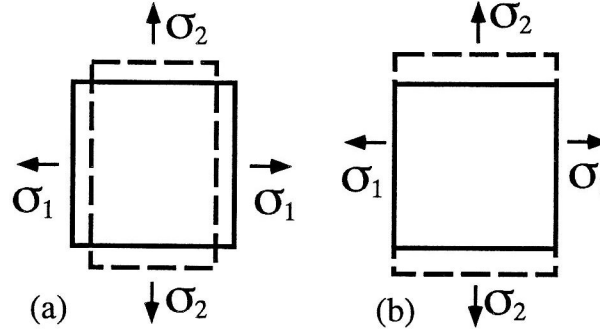


Figure 3. The Unit Cell Set-up. (a) Constant Applied Stress Ratio, (b) Uniaxial Straining

The loading under constant prescribed stress ratio,  $\rho$ , is performed using the modified Riks method as implemented in the finite element code ABAQUS, H.K.S. Inc. (1997). One single four node plane strain element was taken to represent the material cell. The modified Gurson constitutive relation was implemented into a UMAT-subroutine for the finite element code ABAQUS using the method as proposed by Aravas (1987) and Zhang (1994).

### 3 Determination of Parameter Values

Figure 4 depicts the results of the calculations of the behavior of a cell under various stress ratios and uniaxial straining, respectively. Attention is focused on the material traction–separation response in the main loading direction, parallel to  $\sigma_2$ . In all cases as the displacement increases the traction goes through a maximum value and a subsequent reduction in stress carrying capacity is found. The stage of final loss of load carrying capacity associated with the mechanisms of void coalescence as captured by the modified Gurson model is reached at the "knee" of the traction–separation curves.

The maximum traction values of the curves in Figure 4 are identified with the cohesive strength,  $\sigma_{max}$ . The cohesive strength increases nonlinearly as the applied triaxiality is increased. At high values of  $T$  the cohesive strength as predicted for the boundary conditions of constant applied stress ratio approaches the value predicted for the uniaxial straining boundary conditions.

The work of separation, i.e. the values of the integral

$$W = \int_0^{u_2^{sep}} \sigma_2 du_2 \quad (8)$$

are depicted in Figure 5. The limiting values of this integral after final separation is identified with the cohesive energy,  $\Gamma$ . The values of the cohesive energy  $\Gamma/(\sigma_0 D)$  again depend on  $T$ . The values of  $\Gamma/(\sigma_0 D)$  decrease with increasing applied stress triaxialities. At high applied triaxialities  $\Gamma$  is slightly smaller than the value obtained for the boundary conditions of uniaxial straining. The value of the uniaxial straining case is well described by Tvergaard et al. (1992):

$$\Gamma = \frac{1}{2} \sigma_0 D \quad (9)$$

The loading history under imposed uniaxial straining is distinctly different from that under constant imposed stress ratio. It is worth noting the fact, that despite the strongly different loading histories



present in the uniaxial case and for  $T = 4.0$  and  $5.0$  the predicted values of  $\sigma_{max}$  and  $\Gamma$  differ only slightly from the values determined for the uniaxial straining case.

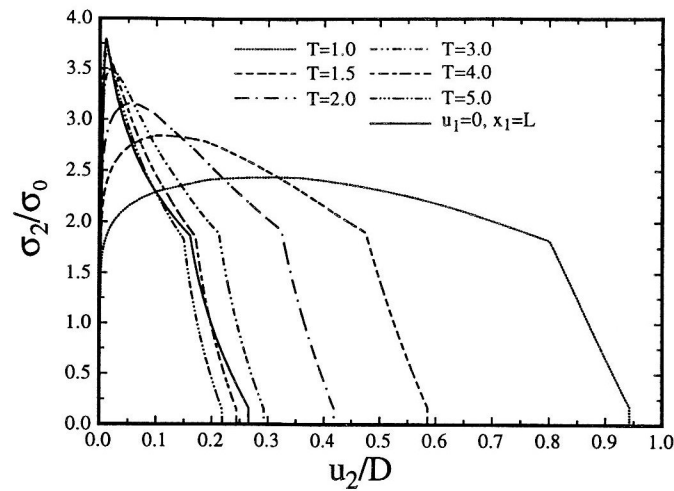


Figure 4. The Traction–Separation Behavior of a Unit Cell Described by the Modified Gurson Relation under Various Constant Applied Stress Ratios and Uniaxial Straining

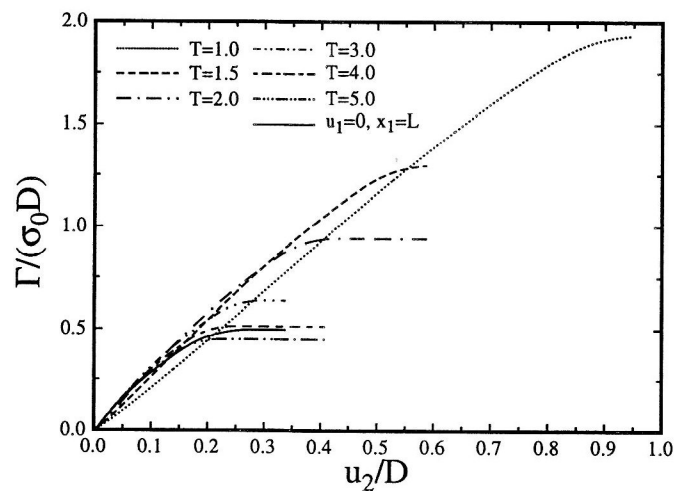


Figure 5. The Evolution of the Work of Separation for the Traction-Separation Curves in Figure 4 for Various Applied Stress Triaxialities and Uniaxial Straining

From the results presented in Figs. 4 and 5 three sets of cohesive zone properties are taken for further considerations; data are taken from loading with  $T = 2.0, 3.0$  and from the case of uniaxial straining,  $CZM\#2, CZM\#3, CZM\#uni$ . These sets of cohesive material properties are summarized in Table 1. The cohesive characteristic lengths,  $\delta$ , is calculated from the values of the cohesive strengths and the cohesive energies by using equation (2).

Name of data set	$\sigma_{max}/\sigma_0$	$\delta/D$	$\Gamma/(\sigma_0 D)$
$CZM\#2$	3.15	0.63	1.12
$CZM\#3$	3.49	0.36	0.71
$CZM\#uni$	3.79	0.23	0.50

Table 1. The Material Data Used in the Calculations

In all the following considerations the differences in shape of the traction–separation curves as depicted in Figure 2 and Figure 4 are disregarded in the determination of the cohesive zone material parameters.

#### 4 Debonding of Two Elastic-Plastic Blocks

The model problem used in the present investigation is the decohesion of two blocks of an elastic-plastic material bonded together without any imperfections. The geometry of the specimen under investigation is depicted in Figure 1a.

The specimen possesses the dimension  $2L \times 2L$  and is deformed under conditions of plane strain. The specimen is located in the  $x_1$ - $x_2$  plane and is assumed to have unit thickness. Symmetry conditions are assumed to prevail and only one quadrant of the specimen is analyzed. The boundary conditions imposed in terms of the boundary displacements,  $U_1, U_2$ , and the tractions,  $T_1, T_2$ , on the quadrant  $x_1 > 0$  and  $x_2 > 0$  are:

$$u_1 = 0 \quad \text{and} \quad T_2 = 0 \quad \text{on} \quad x_1 = 0 \quad (10)$$

$$u_2 = 0 \quad \text{and} \quad T_1 = 0 \quad \text{on} \quad x_2 = 0 \quad (11)$$

$$u_1 = U_1 \quad \text{and} \quad T_2 = 0 \quad \text{on} \quad x_1 = L \quad (12)$$

$$u_2 = U_2 \quad \text{and} \quad T_1 = 0 \quad \text{on} \quad x_2 = L \quad (13)$$

Loading again is performed under constant applied stress ratios,  $\rho$ , equation (6). Now

$$\Sigma_1 = \frac{1}{L + U_2} \int_0^{L+U_2} T_1 dx_2 \quad \dots \quad \text{at} \quad x_1 = L \quad (14)$$

$$\Sigma_2 = \frac{1}{L + U_1} \int_0^{L+U_2} T_2 dx_2 \quad \dots \quad \text{at} \quad x_2 = L \quad (15)$$

For loading under uniaxial straining,  $U_1 = 0$ . The loading under constant stress ratio was again achieved using the "modified Riks method", keeping the ratio  $\Sigma_1/\Sigma_2$  constant.

In the approach using the modified Gurson equation a single row of void containing cells represents the process zone along the  $x_1$ -axis. Due to the symmetry conditions a row of 20 quadrilateral elements of initial height  $D/2$  represent the process zone. The material data used for the description of the process zone in the debonding study are identical to those stated in the previous section.

The material surrounding the region of void containing cells is a non-damageable elastic-plastic material following a  $J_2$ -plasticity theory. Its material properties are taken to be identical with those of the matrix material surrounding the voids in the cell model study. The uniaxial straining properties are given in equation (5). A uniformly spaced mesh region with  $40 \times 39$  equal sized quadrilateral elements is used in the remainder of the quadrant analyzed. The ratio between the process zone height ( $D$ ) and the overall specimen dimension  $L$  was taken to be  $L/D = 100$ . In the presentation of the computational results the curves obtained with process zone modeled by the modified Gurson relation are marked *GTN*.

The alternative approach used is the substitution of the row of void containing cells by a series of cohesive elements. The model contains  $40 \times 39$  continuum elements with elastic-plastic material properties (equation (5)) and 40 cohesive elements at the  $x_1$ -axes. The cohesive elements used in the present calculation possess two integration points.

The implementation of the cohesive elements in the finite element code ABAQUS, H.K.S. Inc. (1997) was performed by the use of user defined elements (UEL) in line with the theory stated in Needleman (1987). Again assuming  $L/D = 100$  the size of the specimen,  $L$ , relative to the cohesive characteristic length,  $\delta$  is  $L/\delta = 159, 275, 538$  for *CZM#2, CZM#3, CZM#uni*, respectively.

#### 5 Results

Decohesion under monotonic loading of the specimen in Figure 1a was calculated for applied constant stress ratios of  $\rho = 0.44, 0.55, 0.67$  and uniaxial straining. In fracture mechanics the term "constraint", i.e. the restriction of deformation, is often used to quantify the conditions under which material failure takes place. For example, an increase in  $\rho$  is equivalent to an increase in constraint. The present simulations of debonding were performed with the aim to see if different descriptions of the process zone can reflect a change in loading conditions in a similar way. For each value of applied stress ratio the process zone was modeled both using the cell model with the material data given in the previous section

and the cohesive zone model with the material data sets  $CZM\#2$ ,  $CZM\#3$ ,  $CZM\#uni$ . Results of the computed overall specimen behavior are depicted in the form of curves of true stress,  $\Sigma_2$ , vs. logarithmic strain,  $E_2 = \ln((U_2 + L)/L)$ . Figures 6 a to d depict this results in the order of decreasing stress ratio. In line with the results published by Needleman (1990a,1990b) it is observed that at high applied stress ratios the debonding process takes place at low overall deformation, Figure 6a,b. The global specimen behavior for uniaxial straining and  $\rho = 0.67$  as predicted by the use of the modified Gurson relation are in very good agreement with the behavior as predicted by the use of the data set  $CZM\#uni$  in the cohesive zone elements. The use of both other data sets,  $CZM\#2$ ,  $CZM\#3$ , leads to lower maximum values of the global stress due to the lower cohesive strengths in these data sets.

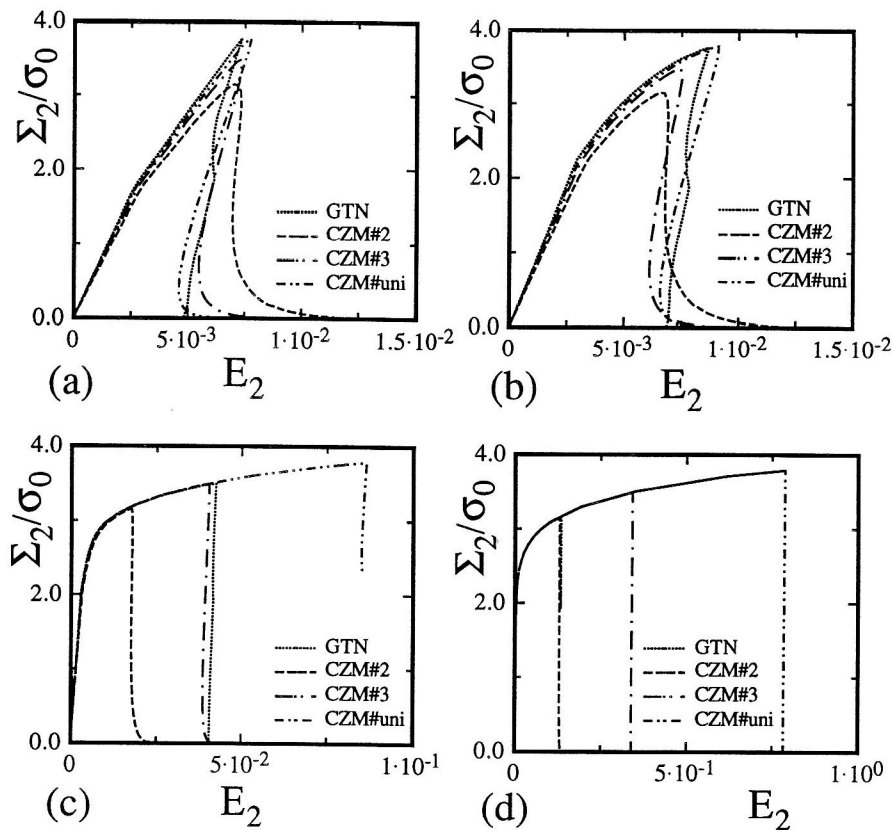


Figure 6. Overall Stress-Strain Curves for Various Loading Situations and Process Zone Descriptions; (a) Uniaxial Straining, (b)  $\rho = 0.66$ , (c)  $\rho = 0.55$ , and (d)  $\rho = 0.44$

The debonding behavior changes considerably when the applied stress ratio is decreased. Two simulations of debonding at low values of  $\rho$  are depicted in Figure 6c and d, for  $\rho = 0.55$  and  $\rho = 0.44$ , respectively. It is worth noting the change in the scale of the strain axis. For  $\rho = 0.55$  and  $\rho = 0.44$  debonding occurs only after considerable deformation of the blocks has taken place. The good agreement between the debonding behavior as predicted by the modified Gurson equation and the use of  $CZM\#uni$  is lost at these stress ratios. It is found that for  $\rho = 0.55$  it is the use of data set  $CZM\#3$  that predicts the debonding in good agreement with the predictions of the modified Gurson model, while for  $\rho = 0.44$  it is the data set  $CZM\#2$ . For both these two cases the use of the data set  $CZM\#uni$  largely overestimates the strains to failure.

Figure 7 depicts the loading-unloading of a point within the block material, again in the order of increasing stress ratio. The trends in the agreement already observed from Figure 6 are mirrored in Figure 7 in the same way. The loading-behavior of a point outside the process zone is again very strongly influenced by the applied stress ratio. Thus, for the approach using the Gurson model the strain to failure depends strongly on  $\rho$ . For the cohesive zone model the predicted failure behavior again strongly depends on the choice of the data set.

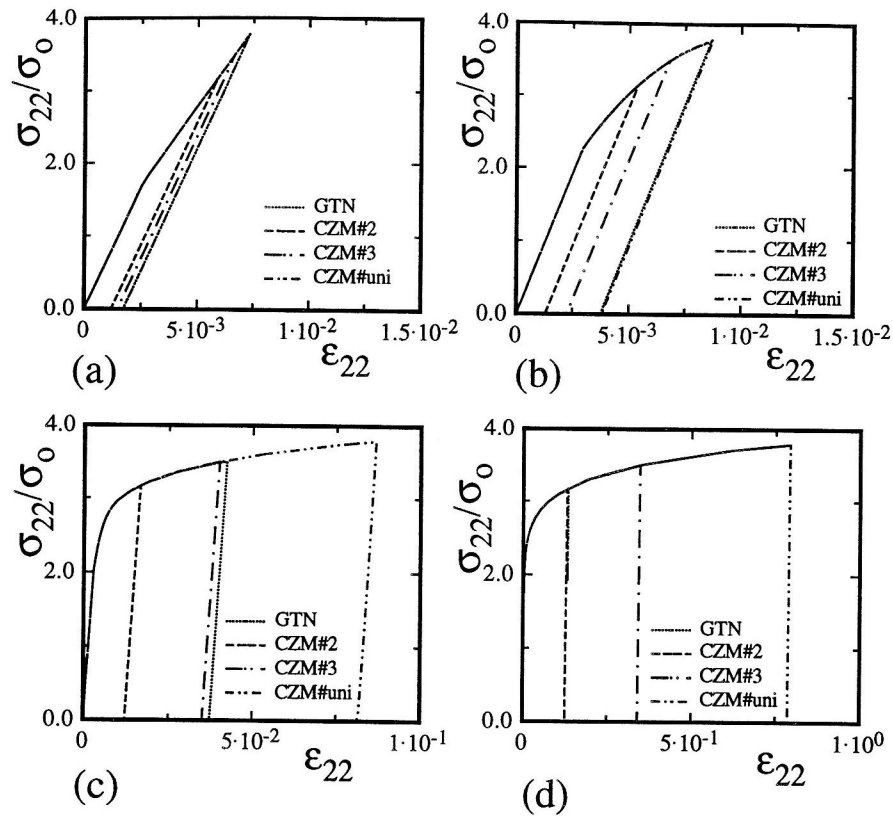


Figure 7. Stress-Strain Curves for a Material Point Outside of the Process Zone for Various Loading Situations and Process Zone Descriptions; (a) Uniaxial Straining, (b)  $\rho = 0.66$ , (c)  $\rho = 0.55$ , (d)  $\rho = 0.44$

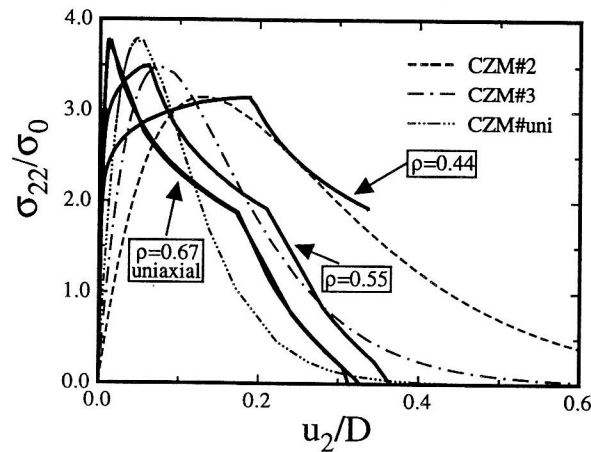


Figure 8. Stress-Strain Curves of a Material Point Inside the Process Zone for Various Loading Situations and Process Zone Descriptions

While the amount of deformation for a point outside the process zone depends strongly on the applied stress ratio this is not the case for the process zone. The loading–unloading behavior of a material point within the process zone is now depicted in Figure 8. The traction separation curves for the cohesive zone model are independent of  $\rho$  while the traction separation curves for the modified Gurson model are definitely dependent on the applied stress ratio. The traction separation curves for the uniaxial straining and the case of  $\rho = 0.67$  are nearly identical despite the difference in the loading history. The maximum stress reached in that case is identical with the cohesive strength in material data set *CZM#uni*. A reduction in  $\rho$  results in a reduction of the maximum of the stress for the process zone modeled by the modified Gurson relation. For  $\rho = 0.55$  the maximum value equals the cohesive strength in data

set *CZM#3* and for  $\rho = 0.44$  for data set *CZM#2*, respectively. Again, the shapes of the traction separation curves are different for the two descriptions of the process zone but this apparently has a minor influence on the overall debonding behavior.

## 6 Conclusion

The debonding behavior of two blocks made of an isotropic elastic-plastic material was analyzed by the two distinctly different approaches of the modified Gurson relation and a cohesive zone model. In the first part of the paper it is shown that in the determination of the cohesive zone parameters special attention has to be devoted to the boundary conditions. The resulting cohesive zone parameters are strongly dependent on the loading conditions as quantified by the parameter stress ratio,  $\rho$ . Thus, it is necessary to test if there exists a set of material data that can describe the debonding of two blocks equally well under all loading situations applied to the blocks. The present investigation demonstrates that it is not possible to choose a set of cohesive surface data that fulfills these requirements. Only for high biaxial loading situations the use of cohesive zone data derived from the cell under uniaxial straining provides an excellent choice. Here one finds good agreement between the resulting overall specimen behavior using the modified Gurson model and the cohesive zone. This holds true even though the shape of the traction separation curves as predicted by the two models are quite different.

The dependence of the failure behavior on the loading conditions becomes very large at low applied stress ratios, i.e. in the case where plastic deformation plays a large role. In that case no unique choice for the cohesive zone parameters can be made to obtain a fit with the predictions from the Gurson model. In that regime the separation behavior as predicted by the Gurson model becomes dependent on the applied stress ratio. That behavior cannot be followed by the present version of the cohesive zone model. Since the behavior of the process zone triggers the overall specimen behavior only rather small changes in the material separation result in large changes in the overall specimen behavior, mainly the strain to failure. Finally, it should be pointed out here that for the choice of the cohesive zone parameters even fulfilling the condition of equal applied stress ratio in the cell model and the decohesion problem does not result in a good agreement between predictions from the cohesive zone model and the modified Gurson model, respectively.

## Literature

1. ABAQUS, Version 5.6., H.K.S. Inc., Pawtucket, U.S.A., (1997).
2. Aravas, N.: On the numerical integration of a class of pressure-dependent plasticity models, *Int. J. Num. Meth. Engng*, 24, (1987), 1395-1416.
3. Barenblatt G.I.: The mathematical theory of equilibrium cracks in brittle fracture, *Adv. Appl. Mech.*, 7, (1962), 55-129.
4. Brocks, W., Sun, D.-Z., Höning, A.: Verification of the transferability of micromechanical parameters by cell model calculations with visco-plastic materials, *Int. J. Plasticity*, 11, 8, (1995), 971-989.
5. Brocks, W., Klingbeil, D., Künecke, Sun, D.-Z.: Application of the Gurson model to ductile tearing resistance, in: *Constraint effects in fracture: Theory and applications*, ASTM STP 144, Kirk, M., Bakker, A., (eds.), Philadelphia, American Society for Testing and Materials, (1995), 232-252.
6. Finot, M., Shen, Y.-L., Needleman, A., Suresh, S.: Micromechanical modeling of reinforcement fracture in particle-reinforced metal-matrix composites, *Metall. Mater. Trans. A*, 25, (1994), 1-18.
7. Hancock, J.W., Cowling, M.J.: Role of state of stress in crack-tip failure processes, *Metal Science*, (1980), 293-304.
8. Koplik, J., Needleman, A.: Void growth and coalescence in porous plastic solids, *Int. J. Solids Structures*, 24, (1988), 835-853.
9. Yuan, H., Lin, G., Cornec, A.: Verification of a cohesive zone model for ductile fracture, *J. Eng. Mater. Tech.*, 118, (1996), 192-200.
10. Needleman, A., Tvergaard, V.: An analysis of ductile rupture in notched bars, *J. Mech. Phys. Solids*, 32, (1984), 461-490.

11. Needleman, A.: A continuum model for void nucleation by inclusion debonding, *J. Appl. Mech.*, 54, (1987) 525-531.
12. Needleman, A.; Tvergaard, V.: An analysis of ductile rupture modes at a crack tip, *J. Mech. Phys. Solids*, 35, (1987), 151-183.
13. Needleman, A.: An analysis of decohesion along an imperfect interface, *Int. J. Fracture*, 42, (1990a), 21-40.
14. Needleman, A.: An analysis of tensile decohesion along an interface, *J. Mech. Phys. Solids*, 38, (1990b), 289-324.
15. Ruggieri, C., Dodds, R.H., Panontin, T.L.: Numerical modeling of ductile crack growth in 3-D using computational cell elements, *Int. J. Fracture*, 82, 1, (1997), 67-95.
16. Siegmund, T., Brocks, W.: Prediction of the work of separation in ductile fracture and implication to the modeling of ductile failure, *Int. J. Fracture*, in print (1998).
17. Siegmund, T., Needleman, A.: A numerical study of dynamic crack growth in elastic-viscoplastic solids, *Int. J. Solids Structures*, 34, 7, (1997), 769-787.
18. Siegmund, T., Needleman, A., Fleck, N.A.: Dynamic Crack Growth Across an Interface, *Int. J. Fracture*, 85 (1997) 381-402.
19. Sun, D.-Z.; Kienzler, R.; Voss, B.; Schmitt, W.: Application of micromechanical models to the prediction of ductile fracture, in: *Fracture mechanics: Twenty-second Symposium (Vol. II)*, ASTM STP 1131, Newman, J.C., Jr., Raju, I.S., Epstein, J.S., (eds.) (1992), 368-378.
20. Tvergaard, V.; Hutchinson, J.W.: The relation between crack growth resistance and fracture process parameters in elastic-plastic solids, *J. Mech. Phys. Solids*, 40, 6, (1992), 1377-1397.
21. Tvergaard, V.; Hutchinson, J.W.: Effect of  $T$ -stress on mode I crack growth resistance in a ductile solid, *Int. J. Solids Structures*, 31, 20-22, (1994), 823-833.
22. Tvergaard, V.; Hutchinson, J.W.: Effect of strain-dependent cohesive zone model on predictions of crack growth resistance, *Int. J. Solids Structures*, 33, 20-22, (1996), 3297-3308.
23. Tvergaard, V.: Model studies of fibre breakage and debonding in a metal reinforced by short fibres, *J. Mech. Phys. Solids*, 41, (1993), 1309-1326.
24. Xia, L., Shih, C.F.: Ductile crack growth – I. A numerical study using computational cells with microstructurally-based length scales, *J. Mech. Phys. Solids*, 43, 2, (1995), 233-259.
25. Xia, L., Shih, C.F.: Ductile crack growth – II. Void nucleation and geometry effects on macroscopic fracture behavior, *J. Mech. Phys. Solids*, 43, 12, (1995), 1953-1981.
26. Zhang, Z.: Ph-D thesis, Norwegian University of Science and Technology, Trondheim, (1994).

---

*Address:* Dr. Thomas Siegmund and Prof. Dr.-Ing. Wolfgang Brocks, Institut für Werkstofforschung, GKSS-Forschungszentrum, D-21502 Geesthacht